

Article

Micro Particle Sizing Using Hilbert Transform Time Domain Signal Analysis Method in Self-Mixing Interferometry

Yu Zhao ^{1,2}, Menglei Zhang ^{1,2}, Chen Zhang ^{1,2}, Wuxiong Yang ^{1,2}, Tao Chen ^{1,2,*},
Julien Perchoux ³ , Evelio E. Ramírez-Miquet ^{3,4}  and Raul da Costa Moreira ³

¹ Institute of Laser Engineering, Beijing University of Technology, Beijing 100124, China; zhaoyuile@bjut.edu.cn (Y.Z.); zhangmenglei@emails.bjut.edu.cn (M.Z.); zchen@emails.bjut.edu.cn (C.Z.); bbgei@bjut.edu.cn (W.Y.)

² Key Laboratory of Trans-Scale Laser Manufacturing Technology, Beijing University of Technology, Ministry of Education, Beijing 100124, China

³ LAAS-CNRS, Université de Toulouse, CNRS, INP, 31400 Toulouse, France; perchoux@laas.fr (J.P.); eramirez@inp-toulouse.fr (E.E.R.-M.); raul.moreira@gmail.com (R.d.C.M.)

⁴ HiFiBiO SAS, Paris 75014, France

* Correspondence: chentao@bjut.edu.cn; Tel.: +86-67393380

Received: 27 November 2019; Accepted: 13 December 2019; Published: 17 December 2019



Abstract: The present work envisages the development of a novel and low-cost self-mixing interferometry (SMI) technology-based single particle sensing system in a microchannel chip for real time single micro-scale particle sizing. We proposed a novel theoretical framework to describe the impulse SMI signal expression in the time domain induced by a flowing particle. Using Hilbert transform, the interferometric fringe number of the impulse SMI signal was retrieved precisely for particle size discrimination. For the ease of particle sensing, a hydrodynamic focusing microfluidic channel was employed by varying the flow rate ratio between the sample stream and the sheath liquid, and the particle stream of a controllable width was formed very easily. The experimental results presented good agreement with the theoretical values, providing a 300 nm resolution for the particle sizing measurement.

Keywords: self-mixing interferometry; microfluidics; hydrodynamic focusing; particle sizing; sensing mechanisms; Hilbert transform

1. Introduction

With the rapid developments in micro-nano technology, a large number of innovative micro- or nanoscale particles have been synthesized that are known to play a crucial role in the biomedical domain such as drug carriers or imaging agents in living tissues. Thus, the characterization of the particle size and other properties remains an extremely fundamental aspect.

As a low-cost, self-aligned, nonintrusive, compact, and reliable sensing approach, self-mixing interferometry (SMI) technology-based microfluidic sensing has gained much attention during the last several decades [1–5]. In such schemes, the laser output amplitude and frequency are modulated when a small fraction of the laser emission is scattered backward by a small particle in the microchannel coupled into the laser cavity. The characteristics of the particle can be extracted from the properties of the SMI modulated signal in both the time-domain and frequency domain.

To date, a great deal of effort has been made in the measurement of the frequency domain. The dynamic scattering (DS) method, as a typical tool for the characterization of the Brownian motion of small particles, can provide a promising assay in SMI-based particle sizing experiments. By measuring

the Doppler power frequency spectrum of scattered light from a particle group, the average particle size can be retrieved. Zakian et al. presented for the first time a theoretical model to describe the frequency-shifted signal power spectrum of a laser source subjected to dynamic scattering light from the particles based on the DS method [6,7]. They demonstrated the possibility of measuring particle sizes ranging from 20 nm to 200 nm. Sudo et al. also successfully implemented particle sizing measurement using the DS method, where the particle dimension and concentration were quantitatively characterized using the Lorentz fitting of the power spectrum of the SMI signal from polystyrene particles of diameters ranging from 20 nm to 500 nm [8,9]. They also reported a forward experimental work by means of an acoustic-optical modulated self-mixing laser metrology for the accurate measurement of diffusion constants [10–13]. More recently, Wang et al. reported a fast and economic home-made signal processing algorithm for nanoparticle size measurement. With a 16 channel analog circuit, the self-mixing AC signal was transformed into DC signals, thus retrieving the size of the nanoparticles [14,15].

However, particle size evaluation techniques in the frequency domain like the DS method are often employed on particle sizes from several to hundreds of nanometers, which are smaller than the laser spot size for a longer autocorrelation time. Moreover, these techniques can only estimate the average particle size of the sample suspension in a high particle number density and low target velocities. For low density particles in the probe volume, the detection was not qualified enough due to a low backscattering efficiency. Single particle detection using the SMI technique still remains challenging, and there are very few reports on single particle detection in a SMI setup [16–18]. Contreras et al. presented a particle size characterization study of single polystyrene spheres with a diameter in several tens of microns in the time domain [17]. They employed a novel SMI scheme with edge-filter enhanced self-mixing interferometry (ESMI), yielding around two orders of magnitude a higher signal-to-noise ratio (SNR) in a lower feedback region even at a 10 m operation distance. Zhao et al. facilitated a robust and real time single particle detection system based on the SMI technique [19]. However, none of the works above-mentioned could measure the particle size with a considerable applied resolution of 1 μm . The existing system still cannot satisfy high throughout real time particle size analysis.

In the present work, we presented a simple and capable SMI-based single particle size characterization method by analyzing the time domain. We proposed a novel conceptual framework of the impulse laser output power signal subject to the feedback modulation from a flowing microparticle, based on the existing well-known theory. In our theoretical model, the relationship between the particle diameter and the interferometric fringe number was investigated. A customized microfluidic chip was designed as a reactor, where a stable particle sample stream was produced to make the single particle pass through the measuring area, and the hydrodynamic focusing performance was tested by varying the flow rate from each inlet. Finally, the SMI signals resulting from the mono particles of different dimensions were acquired and processed by a home-made LabVIEW algorithm involving band-pass filter and Hilbert transform. The resulting interferometric fringe numbers were demonstrated to validate our theory.

2. Theory

When a laser shoots a flowing particle, the laser output power modulation is induced by the interaction between the resulting particle-induced back-scattered light and the laser inner cavity light. In order to describe the laser resonant behavior, here a three-mirror model is shown in Figure 1 [20]. The entire system consists of two cavities, one is the laser cavity of length L_c between the two mirrors (M1, M2) of reflectivity r_1 and r_2 , respectively; the other is the external cavity of length L_{ext} from the laser to the particle in the medium of refractive index n . r_{ext} is the electric field amplitude ratio of the scattered light re-entering the cavity over the original laser light.

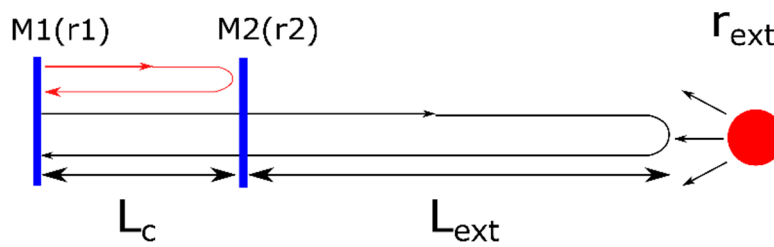


Figure 1. Schematic three-mirror cavity model.

The modulated laser output power $P(t)$ in the presence of the distant target can be expressed using Equations (1) and (2), with the original laser output power P_0 , the modulation index m , and the phase ϕ [21].

$$P(t) = P_0(1 + m \cos \phi) \tag{1}$$

$$m = \frac{4r_{ext}(1 - r_2^2) \tau_p}{r_2 \tau_l} \tag{2}$$

where τ_p is the photon lifetime and τ_l is the round-trip flight time inside the laser cavity. The instantaneous external cavity length, $L_{ext}(t)$ is expressed by the initial length L_0 and the instantaneous displacement ΔL using Equation (3).

$$L_{ext}(t) = L_0 + \Delta L \tag{3}$$

Equation (1) can be rewritten as:

$$P(t) = P_0 \left[1 + m \cos \left(\frac{4\pi L_{ext}}{\lambda} \right) \right] \tag{4}$$

Considering the external cavity length determines the phase ϕ , the displacement ΔL can be measured with a resolution of half wavelength.

$$\phi = \frac{4\pi}{\lambda} (L_0 + \Delta L) \tag{5}$$

Due to the well-known Doppler effect, the frequency of the laser output is shifted by f_D :

$$f_D = \frac{2V \sin \theta}{\lambda} \tag{6}$$

where V is the particle flowing velocity and θ is the incident angle between the laser emission axis and is perpendicular to the plane of the particle flowing direction.

When an individual particle flows through the laser beam emission area from position A to position C, as shown in Figure 2, referring to the laser emission direction, the external cavity facet moves backward from A to B and then forward from B to C, so that ΔL varies the particle diameter D (double the radius r) value during the particle passage. Hence, the particle diameter D can be retrieved from the SMI signal by counting the number of fringes N , with a resolution of half-wavelength order, as shown in Equation (7).

$$D = N \frac{\lambda}{2} \tag{7}$$

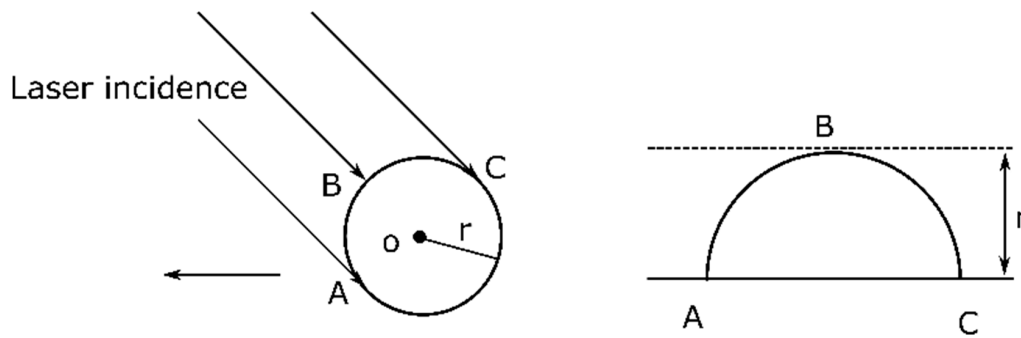


Figure 2. Laser incidence process upon the flowing particle and external cavity length variation ΔL from point A to C.

Based on [22], we propose the following hypothesis: the self-mixing operates on a Gaussian intensity distribution and the self-mixing interference only occurs during the particle passage from point-in-time t_0 , so the SMI signal amplitude also varies as a Gaussian function in the time domain, as shown in Equations (8) and (9).

$$P(t) = P_0 \left[1 + m \cos \left(\phi_0 + \frac{4\pi}{\lambda} \cdot \Delta L \right) \right] \exp \left(-\frac{-(t-t_0)^2}{2w^2} \right) \quad (8)$$

where ϕ_0 is the initial phase. Equation (8) can be extended as:

$$P(t) = P_0 \cdot \exp \left(-\frac{-(t-t_0)^2}{2w^2} \right) + m \cdot P_0 \cos \left(\phi_0 + \frac{4\pi}{\lambda} \cdot \Delta L \right) \cdot \exp \left(-\frac{-(t-t_0)^2}{2w^2} \right) \quad (9)$$

From Equation (9), it can be seen that the SMI signal induced by an individual flowing particle consists of two parts: (1) A Gaussian-shaped waveform pedestal with peak amplitude P_0 and passage duration w (dashed line in Figure 3b) and (2) A sinusoidal oscillation of peak amplitude value mP_0 , also with Gaussian amplitude (Figure 3a,b). This part is the essential result of the interactions inside the cavity between the scattering light from the particle and the initial light containing the particle information such as the particle flowing velocity and particle size. Considering the tiny particle size, r_{ext} is extremely low, so the SMI sensors operate in the weak feedback regime, and the m value is normally in the order of 10^{-6} to 10^{-4} .

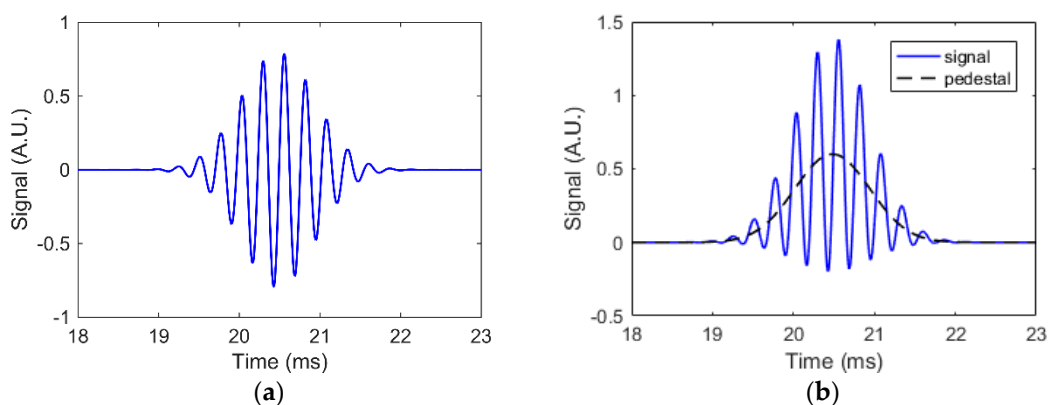


Figure 3. Simulated self-mixing interferometry (SMI) signal in the presence of an individual flowing particle. (a) The Gaussian-shaped sinusoidal SMI signal. (b) The synthesized SMI signal consisting of sinusoidal signal oscillation and pedestal.

3. Experimental Study

Experimental Setup

The experimental measurement setup is illustrated in Figure 4, which consists of three parts: the laser diode based SMI sensor, the microfluidic platform, and the signal processing algorithm.

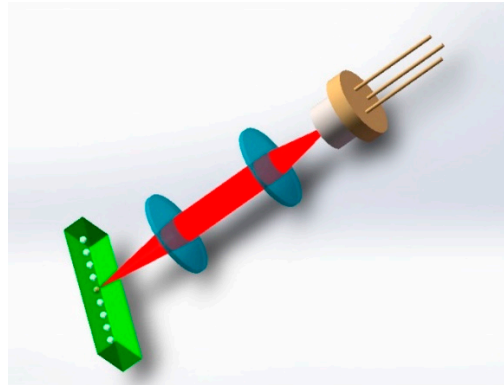


Figure 4. Schematic experimental setup. The system consists of a laser diode, doublet lenses optical arrangement, and microchannel.

The SMI sensor was based on a commercial distributed feedback laser diode (DFB) working at a wavelength of 690 nm (Thorlabs, Newton, US), and the laser operated at a constant voltage through a DC voltage-stabilized source (Rigol, Beijing, CN). The incident angle θ between the laser emission axis and perpendicular to the plane of the channel chip was set to 4° , weighing a satisfying trade-off that allows us to maintain a good signal-to-noise ratio and a sufficient Doppler shift frequency that fitted our acquisition devices. For the laser beam shaping, we used two spherical lenses in the same mode (Thorlabs, Newton, USA) with an 8 mm focal length. The DFB laser and the lens pair were assembled within a cage system (Thorlabs, Newton, USA). Subsequently, the entire optical arrangement was mounted on a 3D translation stage that allowed the adjustment of the focus location. The DFB sensor and the optical arrangement were mounted on a home-made printed circuit board (PCB); by monitoring the embedded photodiode inside the package, the output power fluctuation of the laser diode in the presence of feedback modulation was retrieved. A home-made transimpedance amplifier was employed here to enhance the signal by transforming the photodiode current to voltage. Finally, the signal was acquired using a National Instrument acquisition card (NI-6361 USB) driven by a customized LabVIEW algorithm. The time domain signal was processed by a home-made MATLAB script for burst certification and particle sizing.

In the experimental setup, we applied the single particle sizing measurements using five different diameters polystyrene sphere (PS) aqueous dispersions (Zhongkeleiming, Beijing, CN). The dimension coefficients of variation (CV) values of the particle dimension were better than 3% for each sample. Since the mass density of PS is 1.05 g/cm^3 , similar to that of water, the particles can suspend uniformly in water after being mixed well with an ultrasonic cleaner. As shown in Figure 5, a customized hydrodynamic focusing polydimethylsiloxane (PDMS) microfluidic channel of $100 \mu\text{m}$ thickness was employed as the particle sequence generator chamber and sensing reactor. The dispersions were injected into the channel from the central inlet. Meanwhile, two deionized water fluids were injected using another pump through the other inlets on the left and right side as the sheath flow. Compressed by the double sheath fluids, the particle solution was confined within the center of the channel in the horizontal direction, so the particle group was transformed to a one-by-one sequence after well particle suspension dilution [23]. This allowed for an individual particle to be characterized as they passed through the SMI sensing region at a constant velocity.

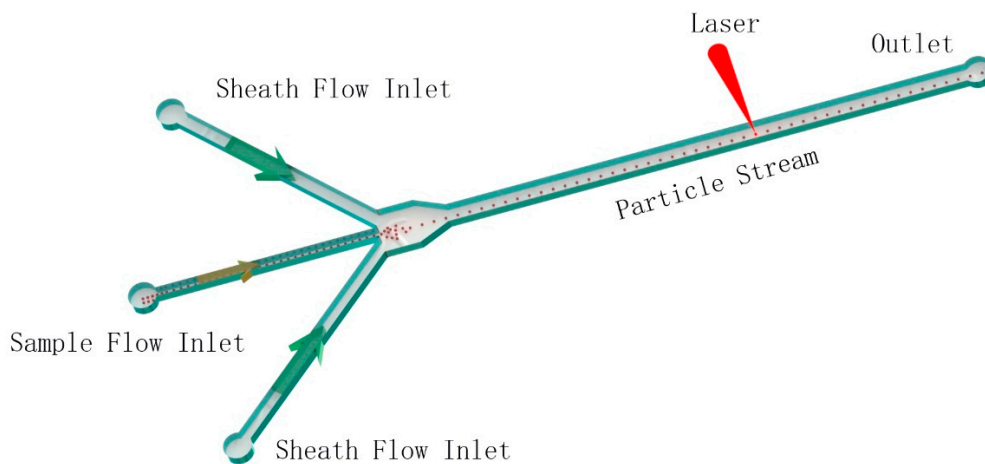


Figure 5. Schematic of the hydrodynamic focusing channel.

In the present work, a home-made data processing algorithm was also proposed. Hilbert transform (HT) is a useful signal processing tool for the description of the complex envelope of a carrier signal. Such a method could represent a signal in its analytical form by performing a 90° phase shift of the original signal over the orthogonal plane without modifying the amplitude, and the phase information is independent of the signal amplitude variations [24]. So far, HT has presented a good performance on SMI signals, as proven in many reports [25–27]. Herein, we employed the HT to unwrap the simultaneous external phase $\phi(t)$ and extract the fringe number correctly.

The transform $HT(u(t))$ was calculated as the convolution of function $u(t)$ with an impulse response function $h(t) = 1/\pi t$.

$$HT(u(t)) = \frac{1}{\pi} \int_{-\infty}^{+\infty} \frac{u(\tau)}{t - \tau} d\tau \quad (10)$$

In this work, the SMI signal $P(t)$ was transformed into a complex analytical form and was expressed as a combination of two orthogonal parts: namely, the real part $\Phi(t)$ and the imaginary part $\Theta(t)$, respectively, and the imaginary part realizes a phase shift of roughly 90° compared to the original SMI signal [28]. The complex form and the phase of the signal can be denoted by the following equations.

$$P(t) = \Phi(t) + j \cdot \Theta(t) \quad (11)$$

$$\Theta(t) = HT(P(t)) \quad (12)$$

$$\phi(t) = \arctan \frac{\Phi(t)}{\Theta(t)} \quad (13)$$

The flow chart of signal acquisition and processing based on the work in [19] is depicted in Figure 6. First, a band-pass filter operated on the raw signal in a certain frequency range (from 1 kHz to 10 kHz) to remove the unwanted high-frequency disturbance from electronic devices and low frequency noise from the signal pedestal in Equation (8). Subsequently, considering the noise floor, a trigger of 200 mV amplitude was applied to the filtered signal. Once the signal amplitude level reached the threshold, the signal sequence in the current acquisition window was saved. Finally, the number of fringes was counted by the Hilbert transformation for single particle characterization.

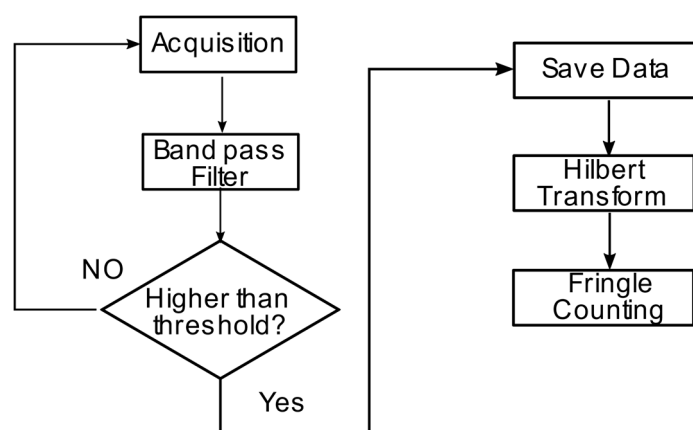


Figure 6. Flow chart drawing of the data acquisition and processing algorithm.

4. Results and Discussion

4.1. Hydrodynamic Focusing of Dye and Particle Streams

First, the hydrodynamic focusing process and laminar flow stability inside the microfluidic chip were observed using an optical microscope. In order to distinguish the boundaries and the widths of the fluids more clearly, 0.1 %wt methylene blue solution was injected into the channel as an indicator. Figure 7 shows the different blue-dyed stream widths of (a) 286 μm , (b) 183 μm , (c) 104 μm , and (d) 51 μm produced by different pumping flow-rate ratios of the analyte/sheath fluid. These photographs indicated well-defined core fluids in the chamber. As the flow rate ratio decreased, the blue inner stream was constricted immediately. All of the streams maintained a constant and straight form over a two-hour period, proving the focusing stability of our channel. Finally, considering the maximum PS dimension ($<10 \mu\text{m}$), we determined the flow rates of the sample and sheath to be 1 and 25 $\mu\text{L}/\text{min}$, respectively, for a 20 μm core fluid width. The maximum Doppler frequency induced by the flowing particle was calculated to be 4.8 kHz by Equation (6).

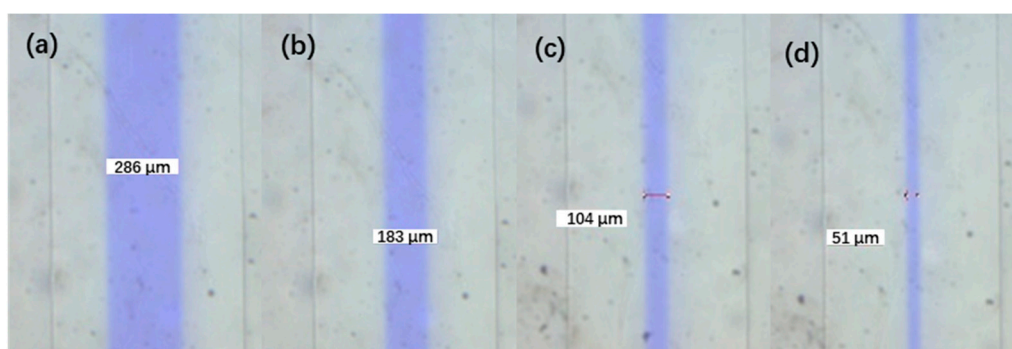


Figure 7. Photographs of the dye fluid in the focusing chamber with sheath-sample-sheath flow rate: (a) 15 $\mu\text{L}/\text{min}$ –20 $\mu\text{L}/\text{min}$ –15 $\mu\text{L}/\text{min}$; (b) 20 $\mu\text{L}/\text{min}$ –10 $\mu\text{L}/\text{min}$ –20 $\mu\text{L}/\text{min}$; (c) 20 $\mu\text{L}/\text{min}$ –5 $\mu\text{L}/\text{min}$ –20 $\mu\text{L}/\text{min}$; (d) 32 $\mu\text{L}/\text{min}$ –4 $\mu\text{L}/\text{min}$ –32 $\mu\text{L}/\text{min}$.

4.2. Single Particle Sizing Measurement

Hundreds of monodispersed signal bursts in different particle sizes were captured and processed by our system as mentioned in the previous section. The sampling frequency and acquisition data number were 500 kHz and 2^{17} , respectively. The data processing results of an 8 μm diameter PS particle are shown in Figure 8. In Figure 8a, the blue and red curves represent the raw SMI signal and the filtered signal in the time domain, respectively. It can be observed that the band-pass filter effectively eliminated the electronic noise, and the impulse waveform evoked from the flowing particle was

distinguished easily. Though the fringes could be observed, there was still some signal perturbation ambiguity in the waveform edge. Thus, after the filter, the phase characterization via Hilbert transform was also employed to extract the fringe number precisely, as shown in Figure 8b, and the fringe number ambiguity was further improved.

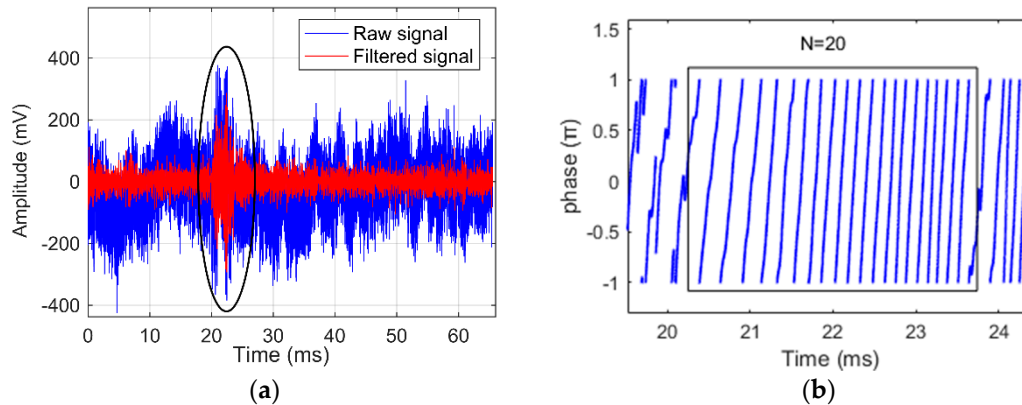


Figure 8. Data processing on the SMI signal from a polystyrene sphere particle of 8 μm diameter. (a) Raw SMI signal (blue) and filtered SMI signal by a home-made band-pass filter (red). (b) Instantaneous phase visualization via Hilbert transform to interfere with fringe number retrieving (in the frame).

We processed 30 signals in the range of 5 μm and 10 μm particle diameters. The distribution of the fringe numbers of the PS particle is shown in Figure 9. It should be emphasized that though the particles were spatially restricted in a small area (20 μm width) inside the hydrodynamic focusing channel center, Doppler frequency shift deviations still existed from 3 kHz to 4.8 kHz. However, according to a given size particle, the fringe number did not vary dramatically at different Doppler frequencies. The fringe number was the eventual characteristic of the given particle.

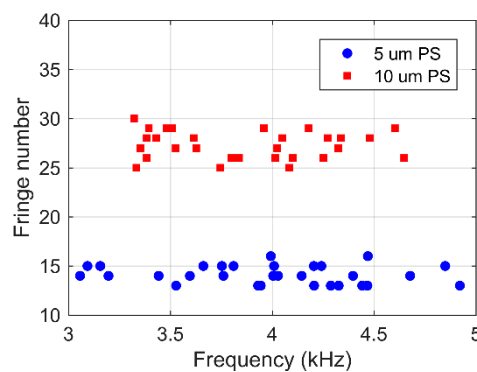


Figure 9. Fringe number trend with SMI signal Doppler frequency of PS particles in different diameters. The blue circles denote 5 μm and the red squares denote 10 μm .

The filtered SMI signal waveforms of different sizes PS samples are illustrated in Figure 10. Well-defined fringe patterns were observed from each particle size, and the waveform performance reasssembled that of the hypothesis above-mentioned in Equation (9) and Figure 3. It was noted that although the 200 nm PS particle was smaller than half of the laser wavelength (350 nm), one integrated waveform could still be presented in the time domain in Figure 10a. Another point worth highlighting is that the signal frequency was not constant during the passage period, and the up-chirp phenomena were observed in the signal bursts, particularly in the bigger particles as shown in Figure 10d. The intervals of the fringes were reduced due to the increase in the frequency. This phenomenon can be explained by the fact that due to the incident angle between the particle flowing direction and the laser axis, the scattering light direction and the Doppler frequency changed during acquisition.

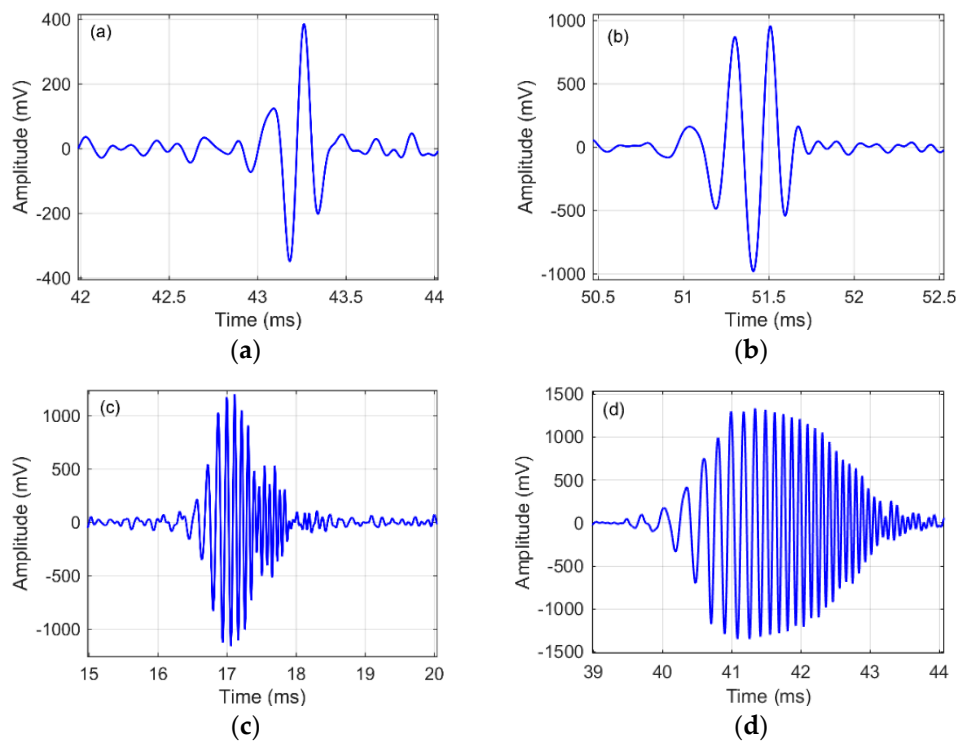


Figure 10. Signal burst of the PS particle in different diameters: (a) 200 nm; (b) 500 nm; (c) 5 μm; (d) 10 μm.

The particle characterization of each particle size was repeated around 100 times, the fringe number trend as a function of the PS particle diameter is depicted in Figure 11. This particle diameter range corresponds to typical human cell dimensions in capillaries. It was observed that the results were in good agreement with the theoretical results calculated by Equation (7), increasing linearly with the particle diameter. The minimal available particle size discrimination by this system was around a half wavelength (~300 nm), and a considerable detection size range from 200 nm to 10 μm was approached, which can be qualified in clinical red blood cell detection.

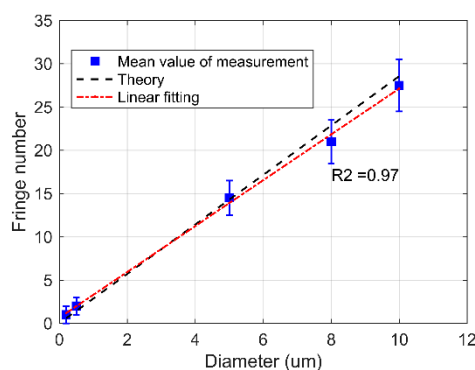


Figure 11. The fringe number of the SMI signal burst as a function of particle diameter. The error bars represent the standard deviation values. The black dashed line denotes the calculation result from Equation (7).

5. Conclusions

In summary, a novel micro scale particle sensing system based on self-mixing interferometry was developed in the present work. By interferometric fringe analysis along with the Hilbert transformation, our system facilitated a fast and precise particle size characterization. A series of

particle sizing experiments using our system were applied herewith in an applicable particle diameter range. The particle sizing results presented good consistency with the theoretical results, thereby successfully proving the efficiency of our method.

We believe that the developed particle sizing approach could be a promising alternative for both chemical analysis and clinical cell or gene characterization. Furthermore, considering the outstanding compactness of the SMI technique, this method can be the first step toward the embedded synthetic particle sensing scheme integrated into Lab-on-a-Chip devices.

Author Contributions: The contribution of the authors to this work is detailed as follows. Investigation, conceptualization and writing, Y.Z., E.E.R.-M., and R.d.C.M.; Experimental validation and visualization, M.Z., C.Z.; Review, W.Y. and J.P.; Supervision, T.C.

Funding: This research was funded by the Beijing Municipal Natural Science Foundation, Grant No. 4194071; the Key Project of Science and Technology of Beijing Municipal Education Commission, Grant No. KZ201910005009, and the Project of Science and Technology of Beijing Municipal Education Commission, Grant No. KM201610005027.

Acknowledgments: The authors acknowledge Yanfeng Gao for their assistance in the PDMS microfluidic channel fabrication processing.

Conflicts of Interest: The authors declare no conflicts of interest.

References

1. Zhao, Y.; Perchoux, J.; Campagnolo, L.; Camps, T.; Atashkhouei, R.; Bardinal, V. Optical feedback interferometry for microscale-flow sensing study: Numerical simulation and experimental validation. *Opt. Express* **2016**, *24*, 23849–23861. [[CrossRef](#)] [[PubMed](#)]
2. Zhao, Y.; Camps, T.; Bardinal, V.; Perchoux, J. Optical Feedback Interferometry Based Microfluidic Sensing: Impact of Multi-Parameters on Doppler Spectral Properties. *Appl. Sci.* **2019**, *9*, 3903. [[CrossRef](#)]
3. Norgia, M.; Pesatori, A.; Rovati, L. Self-mixing laser doppler spectra of extracorporeal blood flow: A theoretical and experimental study. *IEEE Sens. J.* **2012**, *12*, 552–557. [[CrossRef](#)]
4. Campagnolo, L.; Nikolić, M.; Perchoux, J.; Lim, Y.L.; Bertling, K.; Loubiere, K.; Prat, L.; Rakić, A.D.; Bosch, T. Flow profile measurement in microchannel using the optical feedback interferometry sensing technique. *Microfluid. Nanofluid.* **2013**, *14*, 113–119. [[CrossRef](#)]
5. Slot, M.; Koelink, M.H.; Scholten, F.G.; de Mul, F.F.; Weijers, A.L.; Greve, J.; Graaff, R.; Dassel, A.C.; Aarnoudse, J.G.; Tuynman, F.H. Blood flow velocity measurements based on the self-mixing effect in a fibre-coupled semiconductor laser: in vivo and in vitro measurements. *Med. Biol. Eng. Comput.* **1992**, *30*, 441–446. [[CrossRef](#)]
6. Zakian, C.; Dickinson, M.; King, T. Particle sizing and flow measurement using self-mixing interferometry with a laser diode. *J. Opt. A Pure Appl. Opt.* **2005**, *7*, S445–S452. [[CrossRef](#)]
7. Zakian, C.; Dickinson, M.; King, T. Dynamic light scattering by using self-mixing interferometry with a laser diode. *Appl. Opt.* **2006**, *45*, 2240–2245. [[CrossRef](#)]
8. Sudo, S.; Miyasaka, Y.; Otsuka, K.; Takahashi, Y.; Oishi, T.; Ko, J.Y. Quick and easy measurement of particle size of Brownian particles and plankton in water using a self-mixing laser. *Opt. Express* **2006**, *14*, 1044. [[CrossRef](#)]
9. Sudo, S.; Miyasaka, Y.; Kamikariya, K.; Nemoto, K.; Otsuka, K. Microanalysis of Brownian particles and real-time nanometer vibrometry with a laser-diode-pumped self-mixing thin-slice solid-state laser. *Jpn. J. Appl. Phys. Part 2 Lett.* **2006**, *45*, L926. [[CrossRef](#)]
10. Sudo, S.; Miyasaka, Y.; Nemoto, K.; Kamikariya, K.; Otsuka, K. Detection of small particles in fluid flow using a self-mixing laser. *Opt. Express* **2007**, *15*, 8135–8145. [[CrossRef](#)]
11. Otsuka, K.; Ohtomo, T.; Makino, H.; Sudo, S.; Ko, J.Y. Net motion of an ensemble of many Brownian particles captured with a self-mixing laser. *Appl. Phys. Lett.* **2009**, *94*, 241117. [[CrossRef](#)]
12. Ohtomo, T.; Sudo, S.; Otsuka, K. Three-channel three-dimensional self-mixing thin-slice solid-state laser-Doppler measurements. *Appl. Opt.* **2009**, *48*, 609. [[CrossRef](#)] [[PubMed](#)]
13. Sudo, S.; Otsuka, K. Evaluation of resonance phenomena of mechanical oscillator by self-mixing solid-state laser Doppler vibrometry. *Appl. Opt.* **2019**, *58*, 1530. [[CrossRef](#)] [[PubMed](#)]

14. Wang, H.; Shen, J.; Wang, B.; Yu, B.; Xu, Y. Laser diode feedback interferometry in flowing Brownian motion system: A novel theory. *Appl. Phys. B* **2010**, *101*, 173–183. [[CrossRef](#)]
15. Wang, H.; Shen, J. Fast and economic signal processing technique of laser diode self-mixing interferometry for nanoparticle size measurement. *Appl. Phys. B Lasers Opt.* **2014**, *115*, 285–291. [[CrossRef](#)]
16. Herbert, J.; Bertling, K.; Taimre, T.; Rakić, A.D.; Wilson, S. Microparticle discrimination using laser feedback interferometry. *Opt. Express* **2018**, *26*, 25778. [[CrossRef](#)]
17. Contreras, V.; Lönnqvist, J.; Toivonen, J. Detection of single microparticles in airflows by edge-filter enhanced self-mixing interferometry. *Opt. Express* **2016**, *24*, 8886. [[CrossRef](#)]
18. Atashkhoei, R.; Ramirez-Miquet, E.E.; da Costa Moreira, R.; Quotb, A.; Royo, S.; Perchoux, J. Optical Feedback Flowmetry: Impact of Particle Concentration on the Signal Processing Method. *IEEE Sens. J.* **2018**, *18*, 1457–1463. [[CrossRef](#)]
19. Moreira, R.D.C.; Perchoux, J.; Zhao, Y.; Tronche, C.; Jayat, F.; Bosch, T. Single nano-particle flow detection and velocimetry using optical feedback interferometry. In Proceedings of the 2017 IEEE Sensors, Glasgow, UK, 29 October–1 November 2017; pp. 1–3.
20. Wang, W.M.; Grattan, K.T.V.; Palmer, A.W.; Boyle, W.J.O. Self-mixing interference inside a single-mode diode laser for optical sensing applications. *J. Light. Technol.* **1994**, *12*, 1577–1587. [[CrossRef](#)]
21. Servagent, N.; Bosch, T.; Lescure, M. A laser displacement sensor using the self-mixing effect for modal analysis and defect detection. *IEEE Trans. Instrum. Meas.* **1997**, *46*, 847–850. [[CrossRef](#)]
22. Durst, F.; Zare, M. Removal of Pedestals and Directional Ambiguity of Optical Anemometer Signals. *Appl. Opt.* **1997**, *13*, 2562–2579. [[CrossRef](#)] [[PubMed](#)]
23. Chang, C.C.; Yang, R.J. Hydrodynamic Focusing Effect on Two-Unmixed-Fluid in Microchannels. *Int. J. Nonlinear Sci. Numer. Simul.* **2008**, *9*, 213–220. [[CrossRef](#)]
24. Arriaga, A.L. Analysis and Implementation of Algorithms for Embedded Self-mixing Displacement Sensors Design. Ph.D. Thesis, University of Toulouse, Toulouse, France, July 2014.
25. Zhang, Z.; Li, C.; Huang, Z. Vibration measurement based on multiple Hilbert transform for self-mixing interferometry. *Opt. Commun.* **2019**, *436*, 192–196. [[CrossRef](#)]
26. Wei, Y.; Huang, W.; Wei, Z.; Zhang, J.; An, T.; Wang, X.; Xu, H. Double-path acquisition of pulse wave transit time and heartbeat using self-mixing interferometry. *Opt. Commun.* **2017**, *393*, 78–184. [[CrossRef](#)]
27. Zhen, H.; Chengwei, L.; Songquan, L.; Zhenghe, Z.; Dongyu, L. Speckle affected fringe detection based on three envelope extraction for self-mixing displacement measurement. *Opt. Commun.* **2017**, *392*, 100–108. [[CrossRef](#)]
28. Arriaga, A.L.; Bony, F.; Bosch, T. Speckle-insensitive fringe detection method based on Hilbert transform for self-mixing interferometry. *Appl. Opt.* **2014**, *53*, 6954. [[CrossRef](#)]

